Journal of Alloys and Compounds 682 (2016) 753–758

Contents lists available at ScienceDirect

Journal of Alloys and Compounds

journal homepage: http://www.elsevier.com/locate/jalcom

Electric field-assisted flash sintering of $CaCu_3Ti_4O_{12}$: Microstructure characteristics and dielectric properties

Lílian Menezes Jesus [a], Ronaldo Santos Silva [b], Rishi Raj [c], Jean-Claude M'Peko [a, *]

[a] Instituto de Física de São Carlos (IFSC), Universidade de São Paulo (USP), C. Postal: 360, CEP: 13560-970, São Carlos, SP, Brazil
[b] Grupo de Materiais Cerâmicos Avançados, Departamento de Física, Universidade Federal de Sergipe (UFS), CEP: 49100-000, São Cristóvão, SE, Brazil
[c] Department of Mechanical Engineering, University of Colorado at Boulder (UCB), Boulder, CO, 80309-0427, USA

ARTICLE INFO

Article history:
Received 21 November 2015
Received in revised form
29 April 2016
Accepted 1 May 2016
Available online 3 May 2016

Keywords:
Ceramics
Sintering
Microstructure
Dielectric response

ABSTRACT

The electric field-assisted flash sintering method recently introduced in the literature was here considered for producing high-quality $CaCu_3Ti_4O_{12}$ electroceramics, from a powder originally synthesized by a Pechini-derived method and calcined at 800 °C for 2 h. The study included analyzing the dynamics of material shrinkage and densification. With increasing the electric field (E), three distinct regimes were observed: a conventional-like sintering behavior for $E < 15$ V/cm, followed by a region of accelerated (fast-dominated) sintering for $15 \lesssim E < 30$ V/cm, and then the flash-dominated regime, for $E \gtrsim 30$ V/cm, where sintering is not only accelerated but occurs suddenly. In consequence, sintering of the material under field input takes place at furnace temperatures sensibly lower, reaching a value as low as 750 °C for $E = 60$ V/cm versus 1050 °C in conventional processing. The probable physical mechanism behind each regime, including the role of the rise in sample temperature induced by the applied field (Joule heating), is also discussed. Finally, a correlation was found between the microstructure characteristics achieved during sintering and the dielectric response measured.

1. Introduction

Many perovskite (ABO_3-structured) titanates are of great interest because of their exceptional (di)electrical properties and, consequently, use or potential use in several electronic devices [1,2]. This is the case of non-ferroelectric $Ca_{1/4}Cu_{3/4}TiO_3$, or equivalently $CaCu_3Ti_4O_{12}$ (CCTO), which has recently attracted the attention of researchers due to its giant dielectric constant that is stable over a wide range of temperatures [3,4]. This dielectric scenario is partly ideal for the manufacture of high-quality capacitors with, for instance, significantly reduced sizes, as required in microelectronics. It is presently recognized, however, that CCTO has the disadvantage of showing relatively-high dielectric losses. Future works devoted to overcome this limitation would be of great significance for a possible materialization of such applications. Regarding the giant dielectric phenomenon, there seems to be a consensus trend that this arises from the formation of an internal barrier layer capacitor (IBLC) structure in this material, consisting of high-resistivity (insulating-like) grain boundaries versus semiconducting-like grain interior or bulk [5,6]. Next, CCTO was found to show a strong nonlinear current-voltage response, as a result of the existence of a large potential barrier at the grain boundaries [7], a varistor feature that makes it also promising for application in switching and gas-sensing devices.

So far, CCTO electroceramics have been mostly prepared following the conventional solid-state reaction method [4,6,8–11]. These studies have shown that the (micro)structural characteristics as well as (di)electrical properties of CCTO are strongly dependent on the processing conditions (temperatures and annealing times) selected for sintering. This includes observing traces of Cu_XO- and/or TiO_2-rich secondary phases [6,8,9,12,13], the dynamics and kinetics of which are complex, modifying the chemical stoichiometry and (di)electrical response of the grain-boundary as well as the grain-interior micro-regions. Recently, in Ref. [13], the present authors conducted a comparative study on CCTO electroceramics prepared from conventional versus laser sintering, starting from a precursor powder synthesized by a chemical route based on the Pechini method [14], known to enable significantly lower sintering temperatures. It was shown that laser sintering is also an effective procedure for producing high-dielectric constant and fine-grained CCTO electroceramics, with homogeneous microstructures [13]. In

* Corresponding author.
E-mail address: peko@ifsc.usp.br (J.-C. M'Peko).

http://dx.doi.org/10.1016/j.jallcom.2016.05.002
0925-8388/

this approach, however, the sintering area is restricted to the spot of the laser, and sintering larger pieces may imply non-negligible to high processing costs.

An alternative method recently introduced in the literature, and called flash sintering, consists in applying an electric field on the sintering body during thermal treatment, enabling production of high-density ceramics in a matter of seconds, at furnace temperatures well below those required in conventional sintering. This novel method has been successfully applied for the preparation of several materials that include Y_2O_3-doped ZrO_2 [15,16], Co_2MnO_4 [17], MgO-doped Al_2O_3 [18], Gd-doped $BaCeO_3$ [19] and CeO_2 [20], $BaTiO_3$ [21], and TiO_2 [22] electroceramics. This is the processing method we chose in this work to produce high-quality CCTO electroceramics. The conditions of electric field, current density and temperature under which this flash phenomenon develops were explored and are here presented and discussed, together with the effect on microstructure characteristics, correlated with the dielectric response these processed materials finally show.

2. Experimental procedures

$CaCu_3Ti_4O_{12}$ powder was prepared by applying a modified polymeric precursor method [14]. We started with preparation of calcium, copper and titanium citrates, followed by citrate polymerization by adding ethylene glycol, as described in Ref. [13]. The final product was calcined at 800 °C for 2 h, at which conditions synthesis of a single-phase CCTO powder is verified [13]. The powder was uniaxially cold-pressed at 280 MPa in a dog bone-shaped die. Green density of the samples was about 55% of CCTO theoretical density (TD = 5.05 g/cm^3). Electric field-assisted sintering was conducted in a molybdenum di-silicide furnace, following the procedure described in Ref. [18]. The specimen was suspended into the furnace with platinum wires which also served as the field and current carrying electrodes. The furnace temperature was raised at a constant heating rate of 10 °C/min, and the voltage (in the direct current mode) was applied to the specimen when the furnace reached about 500 °C. The current flowing through the specimen increased abruptly at the onset of the flash, at which point the power supply automatically switched from voltage to current control as a current limit of 300 mA (giving a current density of 75 mA/mm^2 in these experiments) was imposed; this led to a fall in applied voltage provided that the conductivity of the specimen continued to increase, as discussed in previous papers (see for example Ref. [23]). The experiments were ended 1 min after the onset of the flash. Because of rapid Joule heating during flash, the specimen temperature in the course of sintering under field input was also measured by using a CLTM-1 Micro-Epsilon optical pyrometer, assuming a specimen emissivity of 0.9 (considered to be a good approximation for most oxide ceramics).

Shrinkage during sintering was measured with a CCD camera that recorded photographs of the specimen at intervals of 1 min before flash, and 1 s just before and during flash. The true linear shrinkage was calculated from $\varepsilon = \ln(L/L_o)$, where L is the time dependent length of the gauge section, and L_o (=2.0 cm) its initial value. The final density of the sintered samples was determined via Archimedes method. For comparison, conventional sintering of some specimens was performed at a temperature of 1050 °C for an identical annealing time of just 1 min. In addition, a set of sintered samples was sputter coated with 10 nm of gold (Au), and their microstructures were analyzed through a field-emission scanning electron microscope (FEG-SEM, FEI Inspect F50), after which the average grain size (AGS) was estimated by applying the linear intercept method [24]. The average particle size of the initial, calcined powder was 0.3 ± 0.1 μm. Finally, for electrical measurements, sintered specimens were cut into rectangular blocks and their surfaces were polished. Platinum electrodes were painted onto both major surfaces, followed by drying at 700 °C for 30 min. Then, measurements of the dielectric permittivity (both real and imaginary parts: $\varepsilon^* = \varepsilon' - j\varepsilon''$, from which the loss tangent can be evaluated as $\tan\delta = \varepsilon''/\varepsilon'$) were carried out at room temperature and frequency range from 0.1 Hz to 2 MHz using an impedance analyzer (HP 4192A). The dimensions of these samples were $6.5 \leq A \leq 11.8$ mm^2 for the painted surfaces and $0.75 \leq h \leq 0.85$ mm for the thickness (i.e., electrodes separation).

3. Results and discussion

Fig. 1 shows the temperature dependence of the true linear strain (ε) of CCTO for all the processed specimens, covering the electric field (E) range from $E = 0$ (conventional processing) to $E = 60$ V/cm. It is noted that sintering under electric field is achieved toward lower furnace temperatures, the only exception applying for $E = 10$ V/cm, for which ε behaved like in conventional sintering: in both cases the sample heating was stopped at 1050 °C (followed by 1 min of annealing and, then, cooling). The final density of all the processed specimens is given in Table 1, noting to range from 90 to 95% TD. For $E > 10$ V/cm, three different regimes were distinguished in the shrinkage curves, as delimited in Fig. 2 for the case of $E = 30$ V/cm: the region we call linear, where ε varies with temperature as in conventional processing ($E = 0$), i.e., where $\Delta\varepsilon = \varepsilon_{\boldsymbol{conv}} - \varepsilon_{\boldsymbol{E}} = 0$ (refer to Fig. 1 for guidance), the FAST (or Type A) region where sintering reveals accelerated and contributes with $\Delta\varepsilon_A$ to the total shrinkage, and then the FLASH (or Type B) region where sintering is virtually instantaneous and contributes with $\Delta\varepsilon_B$ to the total shrinkage. The values of furnace temperature at flash (T_{furn}^{flash}) are also listed in Table 1. The behavior of the linear shrinkage (evaluated as $\Delta\varepsilon = \varepsilon_i - \varepsilon_f$, where ε_i and $\varepsilon_{\boldsymbol{f}}$ refer, respectively, to the initial and final values of shrinkage) as a function of the applied electric field is presented in Fig. 3. Three distinct regions are there identified, namely: the conventional-like region (I) for $E < 15$ V/cm, followed by the FAST-dominated region (II) for $15 \lesssim E < 30$ V/cm, and then the FLASH-dominated region (III) for $E \gtrsim 30$ V/cm. The total shrinkage in either region II or region III is understood to obey $\Delta\varepsilon = \Delta\varepsilon_A + \Delta\varepsilon_B$. Different from the results observed in yttria-doped zirconia, Gd-doped ceria and titania [15,20,22], no clear pure FAST region was verified for sintering of CCTO at $E < 15$ V/cm, noting that the field gap from $E = 10$ to 15 V/cm is only $\Delta E = 5$ V/cm.

Fig. 4 shows the power density (P) dissipated during electric field-assisted sintering of CCTO as a function of the furnace temperature. This physical property, appraised as $P = J\,E$, where J is the measured current density across the sample during sintering, followed a linear-like behavior toward low temperatures when using an Arrhenius-type graph. This can be verified in the figure inset, in which the data have been plotted in terms of conductivity (σ) against $1/T$, where $\sigma = \frac{J}{E} = \frac{P}{E^2}$. This data behavior indicates that the electrical transport in this initial sintering stage can be described by a relation of type $\sigma = \sigma_o \exp\left(-\frac{\Delta Q}{kT}\right)$, where σ_o refers to the pre-exponential factor and ΔQ to the activation energy involved. The values estimated for ΔQ fell within the 1.0–1.3 eV range, comparable to those values found for electrical conduction across grain-to-grain contacts in CCTO electroceramics [8,9]. This is consistent with the assumption that the electrical transport process developing through the sintering body **s**hould be, in this sintering stage, limited by the particle-to-particle contacts along the sample.

In the course of sintering, it is seen in Fig. 4 that P diverges from the low-temperature linear behavior and peaks when flash sintering comes into play. In the following, P reduces to a stable value (steady-like state) as the power supply switched from voltage to

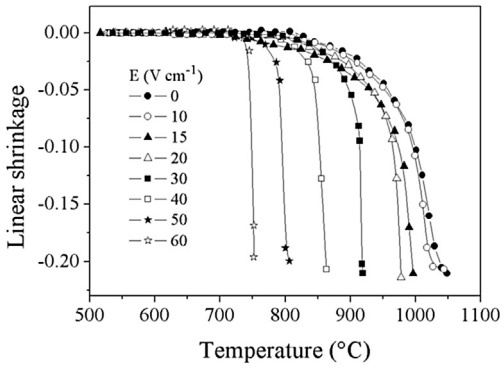

Fig. 1. Temperature dependence of linear shrinkage during conventional and electric field-assisted sintering of CCTO, with a current limit of 300 mA (implying 75 mA/mm^2) and a dwell time of 60 s.

Table 1
Values of applied field (E) and corresponding relative density (ρ_{rel}), furnace (T_{furn}^{flash}) and pyrometer (T_{pyro}^{flash}) temperatures at flash, average grain size (AGS), and dielectric constant (ε') and loss (tanδ) measured at room temperature (RT) and 1 MHz.

E (V/cm)	ρ_{rel} (%TD)	T_{furn}^{flash} (°C)	s (°C)	AGS (μm)	ε' (At RT and 1 MHz)	tanδ
0	94	n/a[a]	n/a[a]	0.64	1821	0.05
10	93	n/a[a]	n/a[a]	1.32	3495	0.09
15	94	995	1120	1.55	4867	0.19
20	95	975	1113	0.98	4292	0.13
30	94	918	1090	0.85	3269	0.07
40	93	860	1053	0.77	2743	0.06
50	91	800	1036	0.70	2629	0.05
60	90	750	1044	0.73	2990	0.06

[a] For these samples the heating process for sintering was stopped at a furnace temperature of 1050 °C, to which corresponded measured pyrometer temperatures of 1050 °C for $E = 0$, as was expected, and 1103 °C for $E = 10$ V/cm; the dwell time at these temperatures was kept to 1 min, as in the flash experiments.

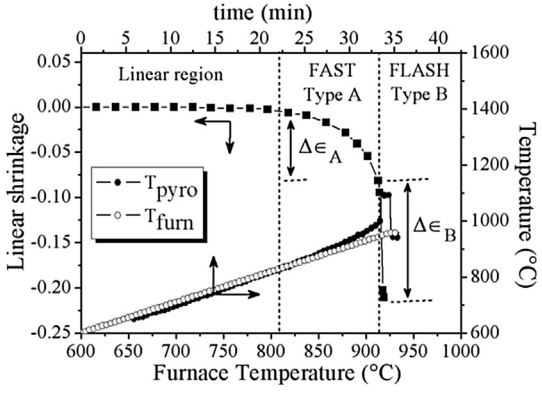

Fig. 2. Dependence of linear shrinkage on furnace temperature (left-hand scale) and time evolution of both furnace and pyrometer temperatures (right-hand scale) during sintering of CCTO under 30 V/cm. Three regions, namely: linear, FAST (or Type A) and FLASH (or Type B) regimes are delimited (see details in the text). FAST and FLASH sintering contribute with, respectively, $\Delta\varepsilon_A$ and $\Delta\varepsilon_B$ to the total shrinkage.

current control, implying, as we earlier mentioned, a voltage drop in order to maintain constant the preset current limit across the sample. Higher current densities were avoided after noting a trend of the sintering body to experience mechanical failure (physical damage caused by electrical breakdown), just as observed in Gd-doped $BaCeO_3$ [19] and $BaTiO_3$ [21]. The sudden increase in power dissipation (nonlinear effect) during flash suggests that the sample temperature may exceed the furnace temperature. For comparison, time evolution of the real (surface) sample temperature, extracted by using a pyrometer directly focused on the sintering body (T_{pyro}), and the furnace temperature (T_{furn}) has been also plotted in Fig. 2 for processing at $E = 30$ V/cm. The curves match at low temperatures, falling within the region we there originally identified as linear regime, toward which changes in furnace and pyrometer temperatures obey $T = T_o + \beta\ t$, with $\beta = 10$ °C/min as was preset. In the FAST regime, T_{pyro} departs from T_{furn} with rising time, the effect of which is suddenly accentuated when FLASH manifests. Once the preset current limit was reached, a stable temperature value was as well reached during the steady state. When the power supply was turned off, both T_{pyro} and T_{furn} coincided again, as expected. The values of specimen temperature resulting from flash (T_{pyro}^{flash}) are also listed in Table 1. T_{pyro}^{flash} is in fact higher than T_{furn}^{flash}, with $\Delta T (= T_{pyro}^{flash} - T_{furn}^{flash})$ increasing systematically when raising E: from $\Delta T = 125$ °C at $E = 15$ V/cm to $\Delta T = 294$ °C at $E = 60$ V/cm. At $E = 10$ V/cm, i.e., conventional-like regime (with sintering finally performed at a furnace temperature of 1050 °C, as for $E = 0$), the difference between pyrometer (specimen) and furnace temperature is 53 °C. It is important mentioning that, since related to surface temperature, T_{pyro}^{flash} may be lower than the real bulk temperature, but closer to this value if compared with the sample temperature measured by the thermocouple positioned near the sintering body, T_{furn}^{flash}.

Back to Figs. 1–3, it seems reasonable stating that in the FAST regime (responsible for $\Delta\varepsilon_A$) Joule heating should contribute to the observed increase in sintering rate, as would be expected. Incidence of the FLASH effect (responsible for $\Delta\varepsilon_B$) is perhaps the most intriguing event when sintering a body under electric field action. Discussion in the literature has been whether the observed increase in sample temperature modulated by Joule heating is as enough as to explain its development, in few minutes to mere seconds as observed here and elsewhere [15–23]. In general, refer also to Fig. 2, it would seem that the sudden increase in sample temperature is the consequence but not (necessarily) the cause of flash sintering instigation. Furthermore, it is seen in Table 1 that T_{pyro}^{flash} is in average lower toward the FLASH- (higher E) than FAST-dominated (lower E) regimes (e.g., $T_{pyro}^{flash} = 1044$ °C at $E = 60$ V/cm versus $T_{pyro}^{flash} = 1120$ °C at $E = 15$ V/cm). In other words, besides the non-negligible influence from Joule heating [23,25,26], there are hints pointing to the possible existence of an additional important contributing mechanism behind flash incidence. In this regard, proposing the generation of an avalanche of defects caused

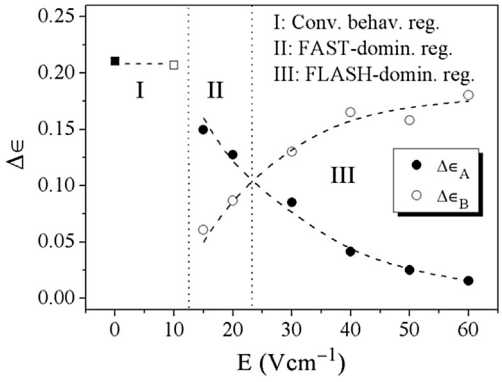

Fig. 3. Partitioning of the linear shrinkage ($\Delta\varepsilon = \varepsilon_i - \varepsilon_f$) attributed to conventional-like behavior (I), FAST- (II) and FLASH-dominated (III) regions. The total shrinkage in either region II or region III is $\Delta\varepsilon = \Delta\varepsilon_A + \Delta\varepsilon_B$. The dashed lines are just a guide for eyes.

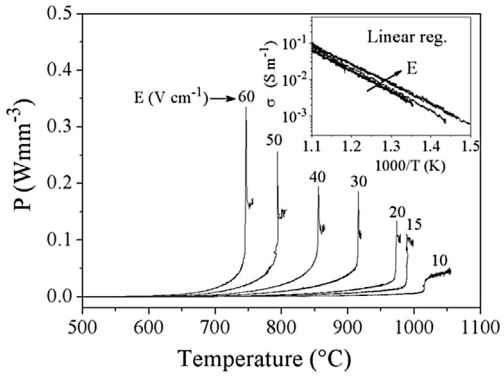

Fig. 4. Temperature dependence of power dissipation during electric field-assisted sintering of CCTO. The behavior toward low temperature (linear region) is shown in the figure inset in terms of Arrhenius plot of conductivity.

by the electric field as the ignition factor of flash appears to make sense, in consonance with observation of an abrupt enhancement in charge diffusion plus mass transport leading to sintering [16,23]. In any case, this is an open debate still needing further experimental evidences from which to draw the valid conclusion.

Fig. 5 illustrates some representative FEG-SEM micrographs of the ceramic samples, showing achievement of dense and homogeneous microstructures. The estimated values of average grain size (AGS) for all the considered sintering conditions are also listed in Table 1, and shown in Fig. 6 for a proper comparative analysis. AGS initially increases with raising E, reaching a maximum value of 1.55 μm at $E = 15$ V/cm, and then systematically decreases for a further increase of E. Like in Fig. 3, the data in this graph have been divided into regions I, II and II. Grain growth in region I, applying for $E < 15$ V/cm, should be ascribed to the increase in sample temperature under electric field input (Table 1). As Fig. 1 suggests, however, the field effect represented in this case solely by Joule heating reveals not enough to promote an enhanced sintering rate during material processing. This should be the consequence of a competition between densification and grain coarsening, bearing in mind that both are proportional to the reciprocal of grain size [27,28]. The result is the observation of a finally conventional-like sintering behavior at $E = 10$ V/cm. This reasoning would also account for the 'anomalous' increase of AGS observed in titania at low fields, toward which shrinkage showed a conventional-like behavior as well, while the sample temperature experienced some important increase [22].

For FAST-dominated sintering, region II applying here for $15 \lesssim E < 30$ V/cm (Fig. 6), the trend of a grain growth retardation has been observed in other materials [15,20,22]. The mechanism behind this result has been proposed, from a thermodynamic viewpoint, to involve a pinning of the grain-to-grain interfaces promoted by a lowering of the interfacial energy under field action [29], or an interaction of the field with the space charge at these micro-regions [30]. For $E = 15$ V/cm, located at the crossover from region I to region II, it seems that influence of the specimen temperature, as in region I, is still responsible for a further slight increase in AGS. Finally, regarding FLASH-dominated sintering, region III applying here for $E \gtrsim 30$ V/cm (Fig. 6), the influence of field on grain size has been found to be variable depending on the material under test [16,20–22]. In this work, AGS experienced a further decrease with raising E, quite similar to what has been observed in Gd-doped ceria [20] and $BaTiO_3$ [21]. It is important to point out that, as also found in $BaTiO_3$, for instance, liquid phase-assisted sintering accompanied by grain growth occurs in CCTO for

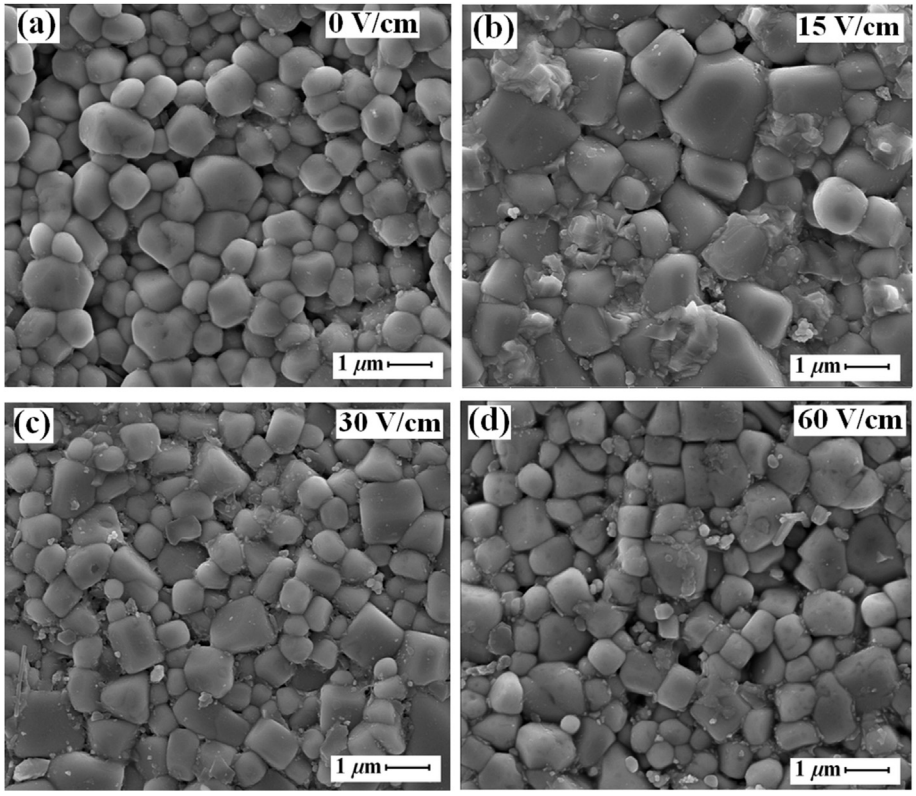

Fig. 5. Representative FE-SEM micrographs of the specimens after (a) conventional ($E = 0$) sintering, and electric field-assisted sintering under (b) $E = 15$ V/cm, (c) $E = 30$ V/cm and (d) $E = 60$ V/cm.

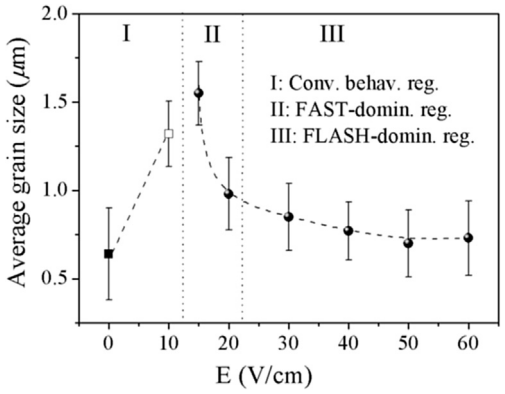

Fig. 6. Variation of the average grain size in the CCTO ceramics upon change in applied electric field. The regions of conventional-like behavior (I), FAST- (II) and FLASH-dominated (III) regimes are delimited. The dashed lines are just a guide for eyes.

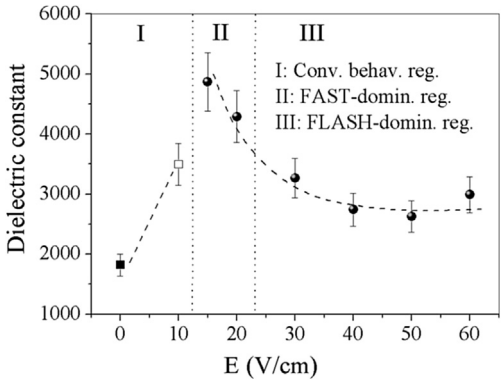

Fig. 8. Variation of the dielectric constant of the CCTO ceramics, as measured at room temperature and 1 MHz, upon applied electric field. The regions of conventional-like behavior (I), FAST- (II) and FLASH-dominated regimes (III) are as well delimited. The dashed lines are just a guide for eyes.

material processing at temperatures, in this case, near to above 1100 °C [13]. Consequently, a decrease in specimen temperature (refer to Table 1) so as avoiding development of such a liquid phase-assisted sintering mechanism might be the reason behind achievement, for $E \gtrsim 30$ V/cm, of CCTO microstructures with a trend of displaying a slightly finer AGS.

Considering that CCTO electroceramics have drawn great attention because showing a high dielectric constant that makes them potential materials for application in electronic devices, we also proceeded with a dielectric characterization of the specimens after conventional as well as electric field-assisted sintering. Fig. 7 illustrates the frequency dependence of dielectric constant (real part of permittivity, ε') for some representative samples (for data clarity), as measured at room temperature. A dielectric dispersion process that involved capacitance values approaching 10^{-8}–10^{-7} F toward the lowest frequencies and 10^{-10} F toward the highest frequencies is observed. These values should be here linked to the dielectric response arising from the material-electrode interfaces and grain boundaries, respectively [31,32]. The figure inset is a magnification of the graph toward high frequencies (showing *plateau*-like dielectric behaviors), from which we chose to compare the 1 MHz-data from all the sintered samples. The extracted values are listed in Table 1, together with the dielectric loss ($\tan\delta$) we measured. Notice that the dielectric constant falls within the 1800–4900 range, values too high for a non-ferroelectric material, reinforcing the hypothesis of their association with the dielectric response likely coming from the grain boundaries. Accessing the bulk dielectric properties from these materials, within the frequency window explored in this work, would require conducting the measurements at lower temperatures; such an experimental approach, followed by a close and much complete dielectric analysis of these CCTO electroceramics, will form the content of a separate contribution. In general, it should be recognized that the dielectric response of electroceramics normally reveals strongly dependent on both measuring frequency and temperature [31–34].

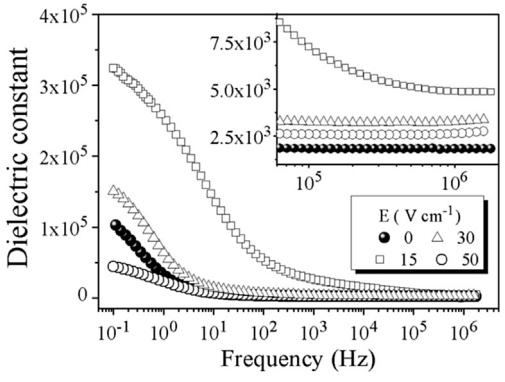

Fig. 7. Representative curves (for data clarity) corresponding to the frequency dependence of the dielectric constant measured in the CCTO ceramics (semi-log graph). The figure inset is a magnification of the graph toward high frequencies.

Fig. 8 depicts the dependence of the dielectric constant from all these CCTO electroceramics, as measured at room temperature and 1 MHz, on the electric field used during sintering. The observed behavior is quite similar to that revealed by AGS in Fig. 6, suggesting that the microstructure characteristics achieved from sintering modify the physical properties these materials finally show. This result can be accounted for by assuming that the microstructures of such ceramics obey a series-layer model applying between grain interior and grain boundaries [31–34]. Accordingly, the individual macroscopic dielectric constant from these micro-regions satisfies $\varepsilon_{gi}^{'(mac)} \cong \varepsilon_{gi}^{'(sp)}$ and $\varepsilon_{gb}^{'(mac)} \cong \varepsilon_{gb}^{'(sp)} D/\delta$, respectively; here "sp" refers to the specific or intrinsic values, D stands for the average grain size (AGS) and δ represents the grain-boundary thickness. From these relations, in which the $D \gg \delta$ approximation has been assumed, only the grain boundaries are expected to show a dielectric constant strongly dependent on grain size. We thus conclude that the dielectric constant of these specimens is (at room temperature and 1 MHz) largely modulated by the grain-boundary response.

4. Conclusions

Electric field-assisted sintering of $CaCu_3Ti_4O_{12}$ (CCTO) was conducted in this work, the results of which can be summarized as follows: (1) sintering is conventional-like for fields (E) < 15 V/cm, becomes accelerated (FAST-dominated effect) for $15 \lesssim E < 30$ V/cm, and then ultra-accelerated (FLASH-dominated effect) for $E \gtrsim 30$ V/cm; (2) both FAST and FLASH events enable CCTO sintering at furnace temperatures considerably lower than in conventional processing; (3) at $E < 15$ V/cm the average grain size increased with field due to Joule heating contribution; (4) toward $E \gtrsim 15$ V/cm the average grain size decreased with the applied field due to (*i*) development of grain-to-grain interface pinning most likely favored by either a lowering of interfacial energy or a field interaction with the grain boundary-related space charge, coupled with (*ii*) body sintering at temperatures low enough to avoid development of a liquid phase-assisted mass transport mechanism for $E \gtrsim 30$ V/cm; (5) the dielectric constant at room temperature and

1 MHz thoroughly reproduced the behavior of the average grain size with varying field, suggesting this physical property to be, in that case, modulated by the dielectric response from grain boundaries; (6) electric field-assisted sintering is here shown to be an alternative and good approach for producing high-quality CCTO electroceramics.

Acknowledgments

The authors are grateful to CAPES, a Brazilian funding agency, for support through grants No. BEX 3276/14-7 and BEX 9291/13-0.

References

[1] A.J. Moulson, J.M. Herbert, Electroceramics: Materials, Properties, Applications, second ed., John Wiley & Sons Ltd., Chichester, 2003.
[2] Y. Xu, Ferroelectric Materials and Their Applications, Elsevier Science Publishers, 1991.
[3] M.A. Subramanian, D. Li, N. Duan, B.A. Reisner, A.W. Sleight, High dielectric constant in $ACu_3Ti_4O_{12}$ and $ACu_3Ti_3FeO_{12}$ phases, J. Solid State Chem. 151 (2000) 323–325.
[4] J. Li, M.A. Subramanian, H.D. Rosenfeld, C.Y. Jones, B.H. Toby, A.W. Sleight, Clues to the giant dielectric constant of $CaCu_3Ti_4O_{12}$ in the defect structure of $SrCu_3Ti_4O_{12}$, Chem. Mater. 16 (2004) 5223–5225.
[5] D.C. Sinclair, T.B. Adams, F.D. Morrison, A.R. West, $CaCu_3Ti_4O_{12}$: one-step internal barrier layer capacitor, Appl. Phys. Lett. 80 (2002) 2153–2155.
[6] R. Schmidt, M.C. Stennett, N.C. Hyatt, J. Pokorny, J.P. Gonjal, M. Li, D.C. Sinclair, Effects of sintering temperature on the internal barrier layer capacitor (IBLC) structure in $CaCu_3Ti_4O_{12}$ (CCTO) ceramics, J. Eur. Ceram. Soc. 32 (2012) 3313–3323.
[7] S.-Y. Chung, I.-D. Kim, S.-J. Kang, Strong nonlinear current-voltage behavior in perovskite-derivative calcium copper titanate, Nat. Mater 31 (2004) 774–778.
[8] R. Löhnert, R. Schmidt, J. Töpfer, Effect of sintering conditions on microstructure and dielectric properties of $CaCu_3Ti_4O_{12}$ (CCTO) ceramics, J. Electroceram. 34 (2015) 241–248.
[9] D. Capsonia, M. Binia, V. Massarotti, G. Chiodelli, M.C. Mozzatic, C.B. Azzoni, Role of doping and CuO segregation in improving the giant permittivity of $CaCu_3Ti_4O_{12}$, J. Solid State Chem. 117 (2004) 4494–4500.
[10] B.A. Bender, M.J. Pan, The effect of processing on the giant dielectric properties of $CaCu_3Ti_4O_{12}$, Mater. Sci. Eng. B 117 (2005) 339–347.
[11] T. Li, R. Xue, J. Hao, Y. Xue, Z. Chen, The effect of calcining temperatures on the phase purity and electric properties of $CaCu_3Ti_4O_{12}$ ceramics, J. Alloys Compd. 509 (2011) 1025–1028.
[12] K.T. Jacob, C. Shekhar, X. Li, G.M. Kale, Gibbs energy of formation of $CaCu_3Ti_4O_{12}$ and phase relations in the system CaO-CuO/Cu_2O-TiO_2, Acta Mater 56 (2008) 4798–4803.
[13] L.M. Jesus, J.C.A. dos Santos, D.V. Sampaio, L.B. Barbosa, R.S. Silva, J.-C. M'Peko, Polymeric synthesis and conventional versus laser sintering of $CaCu_3Ti_4O_{12}$ electroceramics: (micro)structures, phase development and dielectric properties, J. Alloys Compd. 654 (2016), 882–490.
[14] M.P. Pechini, U.S. Patent nº 3,330.697 (1967).
[15] M. Cologna, B. Rashkova, R. Raj, Flash sintering of nanograin zirconia in <5 s at 850 °C, J. Am. Ceram. Soc. 93 (2010) 3556–3559.
[16] J.-C. M'Peko, J.S.C. Francis, R. Raj, Impedance spectroscopy and dielectric properties of flash versus conventionally sintered yttria-doped zirconia electroceramics viewed at the microstructural level, J. Am. Ceram. Soc. 96 (2013) 3760–3767.
[17] A.L.G. Prette, M. Cologna, V.M. Sglavo, R. Raj, Flash-sintering of Co_2MnO_4 spinel for solid oxide fuel cell applications, J. Power Sources 196 (2011) 2061–2065.
[18] M. Cologna, J.S.C. Francis, R. Raj, Field assisted and flash sintering of alumina and its relationship to conductivity and MgO-doping, J. Eur. Ceram. Soc. 31 (2011) 2827–2837.
[19] R. Muccillo, E.N.S. Muccillo, M. Kleitz, Densification and enhancement of the grain boundary conductivity of gadolinium-doped barium cerate by ultra fast flash grain welding, J. Eur. Ceram. Soc. 32 (2012) 2311–2316.
[20] X. Hao, Y. Liu, Z. Wang, J. Qiao, K. Sun, A novel sintering method to obtain fully dense gadolinia doped ceria by applying a direct current, J. Power Sources 210 (2012) 86–91.
[21] J.-C. M'Peko, J.S.C. Francis, R. Raj, Field-assisted sintering of undoped $BaTiO_3$: microstructure evolution and dielectric permittivity, J. Eur. Ceram. Soc. 34 (2014) 3655–3660.
[22] S.K. Jha, R. Raj, The effect of electric field on sintering and electrical conductivity of titania, J. Am. Ceram. Soc. 97 (2014) 527–534.
[23] R. Raj, Joule heating during flash-sintering, J. Eur. Ceram. Soc. 32 (2012) 2293–2301.
[24] American Society for Testing and Materials – ASTM. E1382, Standard Test Methods for Determining Average Grain Size Using Semiautomatic and Automatic Image Analysis, ASTM, 1991. Annual Book of ASTM Standards, v. 03.01.
[25] R.I. Todd, E. Zapata-Solvas, R.S. Bonilla, T. Sneddon, P.R. Wilshaw, Electrical characteristics of flash sintering: thermal runaway of Joule heating, J. Eur. Ceram. Soc. 35 (2015) 1865–1877.
[26] Y. Du, A.J. Stevenson, D. Vernat, M. Diaz, D. Marinha, Estimating Joule heating and ionic conductivity during flash sintering of 8YSZ, J. Eur. Ceram. Soc. 36 (2016) 749–759.
[27] J. Wang, R. Raj, Estimate of the activation energies for boundary diffusion from rate-controlled sintering of pure alumina and alumina doped with zirconia or titania, J. Amer. Ceram. Soc. 73 (1990) 1172–1175.
[28] N.M. Rahaman, Ceramic Processing and Sintering, Chapter 9–12, second ed., Marcel Dekker Inc., New York, NY, 2003.
[29] J. Narayan, Grain growth model for electric field-assisted processing and flash sintering of materials, Scr. Mater. 68 (2013) 785–788.
[30] H. Conrad, Space charge and grain boundary energy in zirconia (3Y-TZP), J. Amer. Ceram. Soc. 94 (2011) 3641–3642.
[31] E. Barsoukov, J.R. Macdonald, Impedance Spectroscopy: Theory, Experiment, and Applications, second ed., John Wiley & Sons, New Jersey, 2005.
[32] M.F. García-Sánchez, J.-C. M'Peko, A.R. Ruiz-Salvador, G. Rodríguez-Gattorno, Y. Echevarría, F. Fernández-Gutierrez, A. Delgado, An elementary picture of dielectric spectroscopy in solids: physical basis, J. Chem. Educ. 80 (2003) 1062–1073.
[33] J.-C. M'Peko, Dynamics of the electrical response of ceramic dielectric materials in the presence of interfacial blocking effects, J. Mater. Sci. Lett. 19 (2000) 1925–1927.
[34] L.M. Nunes, E. Antonelli, M.I.B. Bernardi, T.O. Oladeinde, J.A.S. Caceres, J.-C. M'Peko, How grain boundaries modify the high-temperature dielectric response of ferroelectric electroceramics like $BaTiO_3$? Mater. Res. Bull. 46 (2011) 136–139.